Hybrid materials of MCM-41 functionalized by lanthanide (Tb^{3+}, Eu^{3+}) complexes of modified *meta*-methylbenzoic acid: Covalently bonded assembly and photoluminescence

Ying Li, Bing Yan*

Department of Chemistry, Tongji University, Siping Road 1239, Shanghai 200092, China

Abstract

Novel organic–inorganic mesoporous hybrid materials were synthesized by linking lanthanide (Tb^{3+}, Eu^{3+}) complexes to the mesoporous MCM-41 through the modified *meta*-methylbenzoic acid (MMBA-Si) using co-condensation method in the presence of the cetyltrimethylammonium bromide (CTAB) surfactant as template. The luminescence properties of these resulting materials (denoted as *Ln*-MMBA-MCM-41, *Ln* = Tb, Eu) were characterized in detail, and the results reveal that luminescent mesoporous materials have high surface area, uniformity in the ordered mesoporous structure. Moreover, the mesoporous material covalently bonded Tb^{3+} complex (Tb-MMBA-MCM-41) exhibits the stronger characteristic emission of Tb^{3+} and longer lifetime than Eu-MMBA-MCM-41 due to the triplet state energy of organic legend MMBA-Si matches with the emissive energy level of Tb^{3+} very well.
© 2008 Elsevier Inc. All rights reserved.

Keywords: Covalently bonded mesoporous host; Hybrid material; Lanthanide complex; Luminescence

1. Introduction

Luminescent materials, especially lanthanide phosphors, are applied in many devices of importance [1]. The interest in the photophysical properties of lanthanide complexes which act as optical centers in luminescent hybrid materials has grown considerably since Lehn [2] asserted that such complexes could be seen as light harvest supramolecular devices. Particularly, the design of efficient lanthanide complexes has acquired the attention of many research groups, focusing on the diverse classes of ligands, β-diketones, heterobiaryl ligands, etc. Our research group is focusing on the lanthanide complexes with aromatic carboxylic acid components, bipyridyl or their derivatives [3–5]. In the recent decades, the sol–gel technology has been frequently employed in the synthesis of a significant number of unique attractive organic–inorganic hybrid materials with delicate control and a wide scope of

practical applications [6–9]. Consequently, hybrid silicate materials derived from organo-bridged silsesquioxane precursors with molecular scale homogeneity have now been considerably fabricated by this room temperature method. According to the chemical nature or different synergy between components, hybrids can be categorized into two main classes. The first class concerns all systems where no covalent bond is present between organic and inorganic parts but only weak interactions (such as hydrogen bonding, van der waals force or electrostatic forces). The corresponding conventional doping methods seem hard to prohibit the problem of quenching effect on luminescent centers due to the high vibration energy of the surrounding hydroxyl groups. Therefore, another attracting possibility with regard to the complexation of lanthanide ions using ligands that are covalently fixed to the inorganic networks has emerged. To date, few studies in terms of covalently bonded hybrids with increasing chemical stability have appeared and the as-derived molecular-based materials exhibit monophasic appearance even at a high concentration of lanthanide complexes

*Corresponding author. Fax: +81 21 65982287.
E-mail address:* byan@tongji.edu.cn (B. Yan).

[10–17]. Recently, our group has developed some types of covalently bonded hybrid materials by modifying aromatic acid with modified methyl, carboxyl or hydroxyl groups [18–20] as "molecular bridges". These bridges cannot only develop chelating effects that can bind to lanthanide ions but also link to a silica host with a methylalkoxysilane group.

Due to its peculiar characteristics, large internal surface area and favorable uniformity and easily controlled size of the pore, the ordered mesoporous molecular sieve MCM-41 has attracted considerable interest in physics, chemistry, materials science and other relevant areas [21]. There are many reports on the modification of inorganic mesoporous materials such as MCM-41 silica via post-grafting [22,23] or direct condensing of tetraalkoxysilanes (or organo-functionalized trialkoxysilanes) [24,25], which is also referred to as one-pot synthesis. The latter approach to synthesize MCM-41 was preferred by most researchers because of the simple single-pot synthetic protocol and easy control of organosilane distribution [26]. Besides the advantages of very high surface area, large pore volume and outstanding thermal stabilities, there are a large number of hydroxyl groups in MCM-41, which provide necessary qualification for the modification of inner face and self-assembly of huge guest molecules, namely, providing outstanding hosts for self-aggregation chemistry. Many research efforts, which have focused on preparing the organic/inorganic hybrids through the functionalization of the exterior and/or interior surfaces, prompted the utilization of MCM-41 in many areas [27–30].

Herein, we report a direct synthesis of *meta*-methylbenzoic acid (MMBA)-functionalized MCM-41 mesoporous hybrid material (MMBA-MCM-41), in which MMBA was covalently bonded to the framework of MCM-41 by co-condensation of the modified MMBA (denoted as MMBA-Si) and the tetraethoxysilane (TEOS) using the cetyltrimethylammonium bromide (CTAB) surfactant as template. The luminescent lanthanide (Tb^{3+}, Eu^{3+}) complexes on functionalized MCM-41 with modified MMBA (denoted as *Ln*-MMBA-MCM-41, *Ln* = Tb, Eu) were obtained by introducing Ln^{3+} into the MMBA-MCM-41 hybrid material. Thus, the lanthanide complex *Ln*(MMBA)$_3$ was successfully linked to the framework of MCM-41 via a covalently bonded MMBA group. Full characterization and detail studies of luminescence properties of all these synthesized materials were investigated in relation to guest–host interactions between the organic complex and the silica matrix.

2. Experimental

2.1. Materials

CTAB (Aldrich), TEOS (Aldrich), 3-(methylpropyl)-triethoxysilane (APES, Lancaster), MMBA, and ethanol were used as received. The solvent ether (Et$_2$O) was used after desiccation with anhydrous calcium chloride.

LnCl$_3$ (Ln = Tb, Eu) ethanol solution (EtOH) was prepared as follows: the rare-earth oxide (Tb$_4$O$_7$, Eu$_2$O$_3$) was dissolved in concentrated hydrochloric acid (HCl), and the surplus HCl was removed by evaporation. The residue was dissolved with anhydrous ethanol. The concentration of the rare-earth ion was measured by titration with a standard ethylenediamine tetraacetic acid (EDTA) aqueous solution.

2.2. Synthetic procedures

2.2.1. Synthesis of MMBA-functionalized MCM-41 mesoporous material (MMBA-MCM-41)

The MMBA-Si was prepared as follows: MMBA (1 mmol, 0.136 g) was first converted to acyl chloride by refluxing in excess SOCl$_2$ at the nitrogen atmosphere for 4–5 h. After isolation, the acyl chloride was directly reacted with 3-(methylpropyl)-triethoxysilane (APES) (1 mmol, 0.221 g) in ethyl ether in presence of triethylamine. The mixture was heated at 65 °C in a covered flask for approximately 12 h at the nitrogen atmosphere. After isolation and purification, a yellow oil sample MMBA-Si was obtained. Anal: calcd. for C$_{17}$H$_{29}$NO$_4$Si: C: 60.17; H: 8.55; N: 4.13; Found: C, 60.12; H, 8.49; N, 4.11%. ^{1}H NMR (CDCl$_3$): δ 7.78(1H, s), 7.76(1H,s), 7.41(2H,s), 3.80(1H,t), 3.45(10H,m), 3.10(2H,s), 2.33(3H,d), 1.57(4H,s), 1.19(2H,s), 0.59(3H,s). ^{13}C NMR (CDCl$_3$): δ 167.3(C$_7$), 137.6(C$_1$), 133.7(C$_3$), 130.6(C$_6$), 129.4(C$_4$), 128.4(C$_5$), 126.2(C$_2$), 72.5–71.4(C$_9$–C$_{10}$), 69.9(C$_{11}$), 55.9(C$_8$), 49.8(C$_{12}$), 18.4(C$_{13}$).

The mesoporous material MMBA-MCM-41 was synthesized as follows: CTAB (1.1 g) was dissolved in concentrated NH$_3$·H$_2$O (12 mL), to which deionized water (26 mL), TEOS (5.5 mL), and MMBA-Si were added with the following molar composition: 0.12 CTAB:0.5 NH$_3$·H$_2$O:0.96 TEOS:0.04 MMBA-Si:58.24 H$_2$O. The mixture was stirred at room temperature for 24 h and transferred into a Teflon bottle sealed in an autoclave, which was then heated at 100 °C for 48 h. Then the solid product was filtrated, washed thoroughly with deionized water, and air-dried for 12 h at room temperature. Removal of the surfactant CTAB was conducted by Soxhlet extraction with ethanol for 2 days to give the sample denoted as MMBA-MCM-41.

2.2.2. Synthesis of MCM-41 mesoporous material covalently bonded with the lanthanide (Ln^{3+}) complexes (denoted as Ln-MMBA-MCM-41, Ln=Tb, Eu)

The sol–gel-derived mesoporous hybrid material was prepared as follows: while being stirred, MMBA-MCM-41 was soaked in an appropriate amount of LnCl$_3$ ethanol solution with the molar ratio of Ln^{3+}: MMBA-Si being 1:3. The mixture was heated at 75 °C under reflux for 12 h, followed by filtration and extensive washing with EtOH. The resulting materials *Ln*-MMBA-MCM-41(Eu^{3+}, Tb^{3+}) was dried at 60 °C under vacuum overnight and the lanthanide ion content of the materials was 1.26% (mol%). The hybrid mesoporous *Ln*-MMBA-MCM-41 product was obtained (as outlined in Fig. 1).
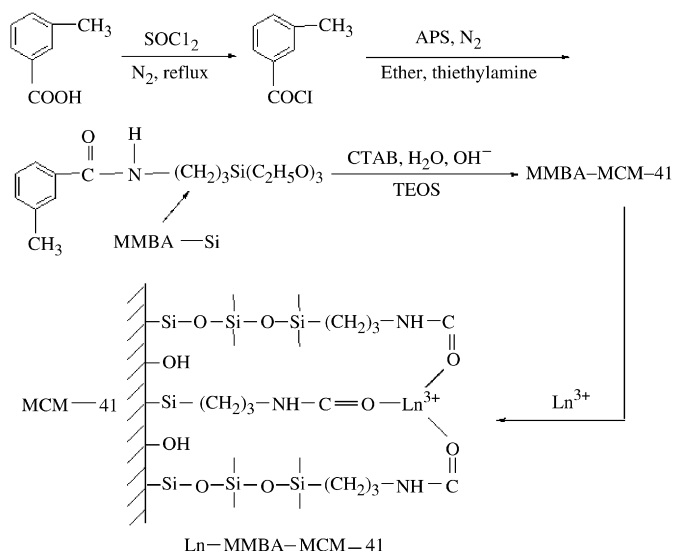
Fig. 1. The scheme for the synthesis procedure and predicted structure of *Ln*-MMBA-MCM-41 (*Ln* = Tb, Eu).

2.3. Characterization

IR spectra were measured within the 4000–400 cm^{-1} region on an infrared spectrophotometer with the KBr pellet technique. ^1H NMR spectra were recorded in $CDCl_3$ on a Bruker AVANCE-500 spectrometer with tetramethylsilane (TMS) as internal reference. Elemental analyses (C, H, N) were determined with an Elementar Cario EL elemental analyzer. The ultraviolet absorption spectra were taken with an Agilent 8453 spectrophotometer. X-ray powder diffraction patterns were recorder on a Rigaku D/max-rB diffractometer equipped with a Cu anode in a 2θ range from $0.6°$ to $6°$. Nitrogen adsorption/desorption isotherms were measured at the liquid nitrogen temperature, using a Nova 1000 analyzer. Surface areas were calculated by the Brunauer–Emmett–Teller (BET) method and pore size distributions were evaluated from the desorption branches of the nitrogen isotherms using the Barrett–Joyner–Halenda (BJH) model. The fluorescence excitation and emission spectra were obtained on a Perkin-Elmer LS-55 spectrophotometer. Luminescence lifetime measurements were carried out on an Edinburgh FLS920 phosphorimeter using a 450 W xenon lamp as excitation source. Scanning electronic microscope (SEM) was measured on Philip XL30 operated. Transmission electron microscope (TEM) experiments were conducted on a JEOL2011 microscope operated at 200 kV or on a JEM-4000EX microscope operated at 400 kV.

3. Results and discussion

3.1. Characterization and physical properties of meta-methylbenzoic acid-functionalized mesoporous silica MCM-41

The presence of the organic ligand MMBA covalently bonded to the mesoporous MCM-41 was characterized by

IR and UV absorption spectra. The IR spectra for MMBA, MMBA-Si, and MMBA-MCM-41 are shown in Fig. 2. The occurrence of the grafting reaction was supported by the bands located at 1634 cm^{-1}, which originated from the absorption of amide groups (–CONH–). In addition, a series of strong bands at around 2975, 2928, and 2884 cm^{-1} are due to the vibrations of methylene—$(-CH_2)_3$—in the APES, proving that 3-(methylpropyl)-triethoxysilane has been successfully grafted on to MMBA [31]. In addition, the formation of the Si–O–Si framework is evidenced by the bands located at 1087 cm^{-1} (ν_{as}, Si–O), 805 cm^{-1} (ν_s, Si–O), and 466 cm^{-1} (δ, Si–O–Si) (ν represents stretching, δ in plane bending, s symmetric, and as asymmetric vibrations), indicate the absorption of siloxane bonds. Furthermore, the peaks at 1622 and 1383 cm^{-1} originating from –CONH– group of MMBA-Si, can also be observed in hybrid mesoporous material MMBA-MCM-41, which is consistent with the fact that the MMBA group in the framework remains intact after both hydrolysis-condensation reaction and the surfactant extraction procedure [28].

Fig. 3 shows the UV absorption spectra of MMBA, MMBA-Si and MMBA-MCM-41. Comparing the absorption spectrum of MMBA-Si with that of MMBA, we can see a blue-shift of the major π–π^* electronic transitions from 246 to 219 nm, and the appearance of the new peak centered at 242 nm, indicating that modification of MMBA, which was grafted by 3-(methylpropyl)-triethoxysilane, influences its corresponding absorption.

3.2. Characterization and physical properties of lanthanide (Ln^{3+}) complexes covalently bonded to MMBA-functionalized mesoporous MCM-41

The small-angle X-ray diffraction (SAXRD) patterns and nitrogen adsorption/desorption isotherms are popular
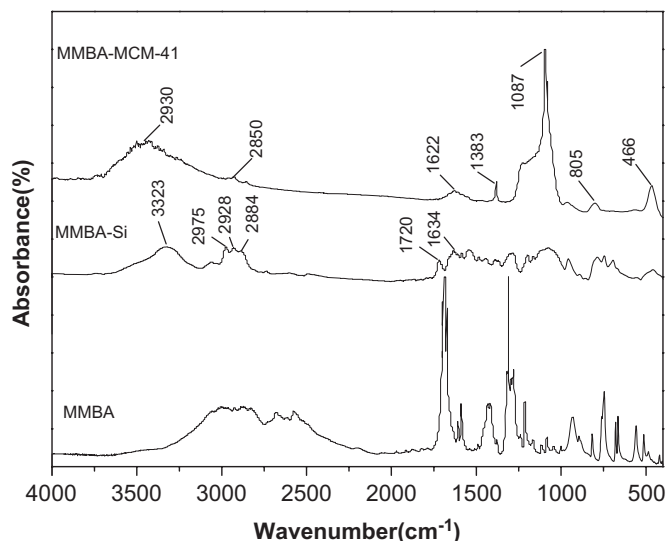

Fig. 2. IR spectra of MMBA-Si and covalently bonded hybrid mesoporous material MMBA-MCM-41.
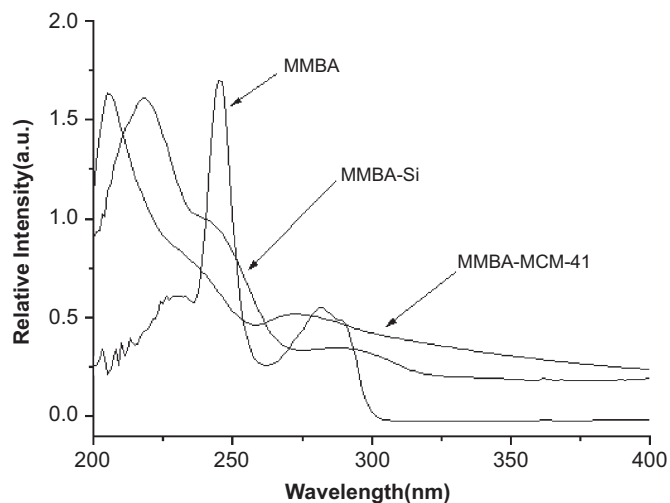
Fig. 3. UV absorption spectra for *meta*-methylbenzoic acid, MMBA-Si and MMBA-MCM-41.

Fig. 4. XRD patterns of MCM-41 (a), MMBA-MCM-41 (b), Tb-MMBA-MCM-41 (c), and Eu-MMBA-MCM-41 (d).

and efficient methods to characterize highly ordered mesoporous material with hexagonal symmetry of the space group *p6mm*. The SAXRD patterns of pure MCM-41(a) mesoporous silicon (which is prepared according to Refs. [32,33]), MMBA-MCM-41(b) and two kinds of lanthanide complexes functionalized MCM-41 materials are presented in Fig. 4. For all materials, the patterns clearly show the order of the hexagonal array of the MCM-41 structure and exhibit distinct Bragg peaks in the 2θ range of 0.6–6°, which can be indexed as (100), (110), and (200) reflections. Compared with the SAXRD pattern of MCM-41, the covalent grafting of the corresponding organosiloxanes to the silica walls do not induce considerable lattice shrinkage, as indicated by the similar d_{100} spacing values of *Ln*-MMBA-MCM-41 (*Ln* = Tb, Eu) (see Table 1), indicating that the framework hexagonal ordering has been retained very well upon the introduction of Ln^{3+} complexes. In addition, it is worth noting that lanthanide complex functionalized materials *Ln*-MMBA-MCM-41 appear decreasing in diffraction intensity as compared with MCM-41, which is probably due to the presence of guest moieties inside the pore channels of host MCM-41 material, resulting in the decrease of the mesoporous order, but not the collapse in the pore structure of mesoporous materials [29]. The hexagonal symmetry of Tb-MMBA-MCM-41 inferred from SAXRD is also in agreement with the HRTEM investigation. HRTEM image of the mesoporous material is given in Fig. 5 and confirms the suggested *p6mm* symmetry, indicating that after the complexation process the mesoporous structure of Tb-MMBA-MCM-41 can be substantially conserved.

The N_2 adsorption–desorption isotherm and pore size distribution for MCM-41, MMBA-MCM-41, Tb-MMBA-MCM-41, and Eu-MMBA-MCM-41 samples are shown in Fig. 6. They all display Type IV isotherms with H1-type hysteresis loops at low relative pressure according to the IUPAC classification [34–37], characteristic of mesoporous
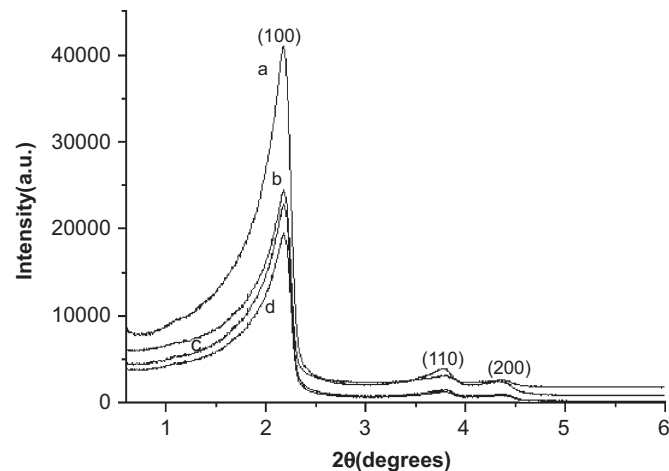
Table 1
Textural data of MCM-41, MMBA-MCM-41-Tb, and MMBA-MCM-41-Eu[a]

Sample	d_{100} (nm)	S_{BET} (m^2/g)	V (cm^3/g)	D_{BJH} (nm)	a_0
MCM-41	4.07	1028.11	0.77	3.43	4.70
Tb-MMBA-MCM-41	3.85	534.50	0.52	2.70	4.45
Eu-MMBA-MCM-41	3.84	516.60	0.50	2.71	4.43

[a] d_{100} is the $d(100)$ spacing, a_0—cell parameter ($a_0 = 2 d_{100}/3$), S_{BET}—the BET surface area, V—the pore volume, and D—the pore diameter.
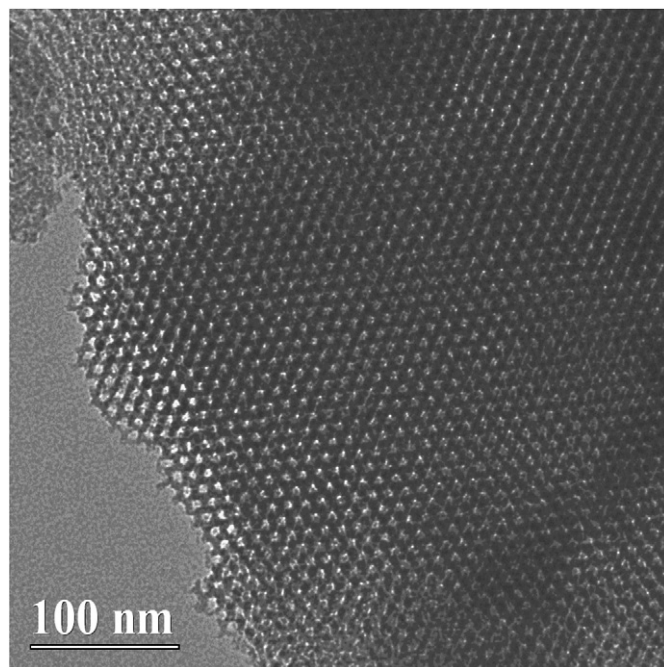

Fig. 5. HRTEM image of Tb-MMBA-MCM-41 recorded along the [100] zone axe.

materials with highly uniform size distributions. From the two branches of adsorption–desorption isotherms, the presence of a sharp adsorption step in the P/P_0 region from 0.3 to 0.5 and a hysteresis loop at the relative pressure $P/P_0 > 0.45$ shows that all materials process a well-defined array of regular mesopores. The specific area and the pore size have been calculated by using BET and BJH methods, respectively. The structure data of all these mesoporous materials (BET surface area, total pore volume, pore size, etc.) were summarized in Table 1. It can be clearly seen that mesoporous materials MMBA-MCM-41 and *Ln*-MMBA-MCM-41 exhibit a smaller specific area and a slightly smaller pore size and pore volume in comparison with those of pure MCM-41, which might be due to the presence of organic ligand MMBA on the pore surface and the co-surfactant effect of MMBA-Si, which interacts with surfactant and reduces the diameter of the micelles [38,39]. This further confirmed that $Ln(MMBA-Si)_3$ complexes covalently bonded with the mesoporous silica MCM-41.

The IR spectra of MCM-41, Eu-MMBA-MCM-41, and Tb-MMBA-MCM-41 are shown in Fig. 7. In the MCM-41 host material, the evident peaks appearing at $1000–1250\,cm^{-1}$ range are due to asymmetric Si–O stretching vibration modes (ν_{as}, Si–O), and the peak at $805\,cm^{-1}$ can be attributed to the symmetric Si–O stretching vibration (ν_s, Si–O). The Si–O–Si bending vibration (δ, Si–O–Si) can also be observed at $465\,cm^{-1}$, and the bands at $968\,cm^{-1}$ is associated with silanol (Si–OH) stretching vibrations of surface groups [40]. In addition, the presence of hydroxyl can be clearly evidenced by the peak at $3462\,cm^{-1}$. Compared with MCM-41, the hybrid mesoporous materials *Ln*-MMBA-MCM-41 ($Ln =$ Tb, Eu) not only exhibit the similar infrared absorption bands as the silica framework but also the peaks at around $1380\,cm^{-1}$ range, which just originated
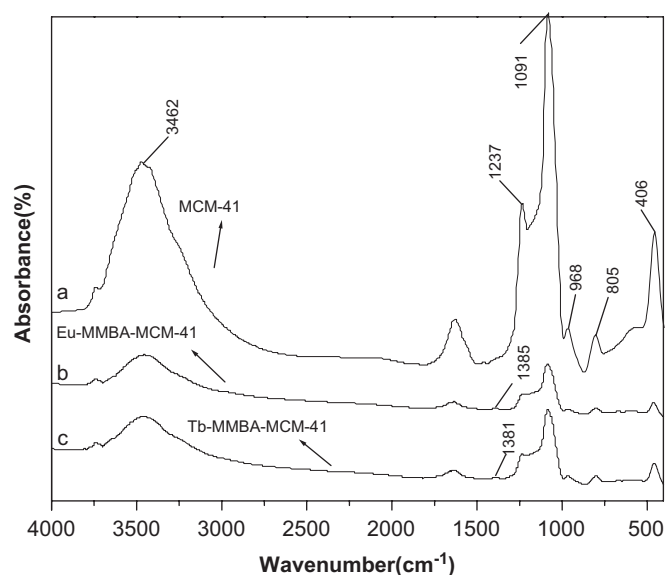

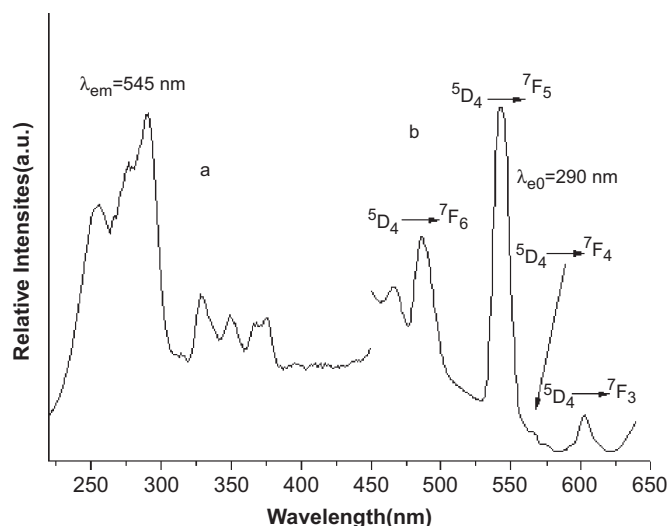Fig. 7. IR spectra of MCM-41 (a), Eu-MMBA-MCM-41 (b), and Tb-MMBA-MCM-41 (c).

Fig. 8. Excitation (a) and emission (b) spectra of Tb-MMBA-MCM-41 hybrid material.

from the –CONH– group of MMBA-Si, indicating that MMBA-Si has been grafted onto the wall of MCM-41.

3.3. Photoluminescent properties

Fig. 8 and Fig. 9 show the excitation and emission spectra of pure $Tb(MMBA)_3$ complex and Tb-MMBA-MCM-41 mesoporous material. The excitation spectrum (Fig. 8a), monitoring the strongest emission band of the Tb^{3+} ion at 545 nm, presents a large broad band between 225 and 325 nm in Tb-MMBA-MCM-41 attributed to the light absorption by the charge transfer state (CTS) of Tb–O. Compared with the pure $Tb(MMBA)_3$ complex (Fig. 9a), the excitation becomes narrower and the maximum excitation wavelength shifts from 357 to
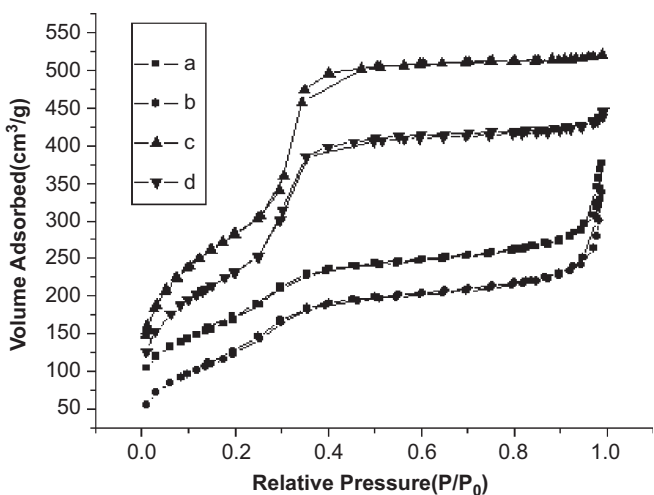

Fig. 6. N_2 adsorption/desorption isotherms of Tb-MMBA-MCM-41 (a), Eu-MMBA-MCM-41 (b), MCM-41 (c), and MMBA-MCM-41 (d) hybrid materials.

290 nm for Tb-MMBA-MCM-41. The blue-shift of the excitation bands as the introduction of Tb^{3+} complex into the mesoporous material is due to a hypsochromic effect resulting from the change in the polarity of the environment surrounding the terbium complex in the mesoporous material [30]. Besides, the sharp excitation peaks in the long wavelength region around 400 nm can be ascribed the characteristic $f–f$ transition of Tb^{3+}. From the emission spectra (Fig. 8b), characteristic Tb^{3+} ion emissions are observed. Three bands can be clearly seen in the 450–650 nm range, which are assigned to the $^5D_4 \rightarrow {}^7F_J$ ($J = 6–4$) transitions at 487, 544, 582, 620 nm, respectively. As a result, the strong green luminescence was observed in the emission spectra, which indicated that the effective energy transfer took place between the modified MMBA and the chelated Tb^{3+} ions. The hybrid mesoporous material Tb-MMBA-MCM-41 shows relatively strong emission due to the chemically covalently bonded molecular Si–O network structure between the complex and the mesoporous silica. Furthermore, the luminescence intensities of the $^5D_4 \rightarrow {}^7F_5$ transition for pure $Tb(MMBA)_3$ complex and Tb-MMBA-MCM-41 were compared. The relative intensity of Tb-MMBA-MCM-41 mesoporous material is stronger than that of pure $Tb(MMBA)_3$ complex, which indicates that the MCM-41 is an excellent host for the luminescence $Tb(MMBA)_3$ complex.

The excitation and emission spectra of Eu-MMBA-MCM-41 are given in Fig. 10. The excitation spectrum was obtained by monitoring the emission of Eu^{3+} at 613 nm and dominated by a distinguished band centered at 324 nm. As shown in Fig. 10a, the excitation spectrum of the mesoporous material Eu-MMBA-MCM-41 exhibits CTS of Eu–O from 220 to 350 nm, and a peak at 392 nm can be observed due to the $f \rightarrow f$ absorption transition ($^7F_0 \rightarrow {}^5D_2$) of Eu^{3+} ion. The emission lines of Eu-MMBA-MCM-41 (Fig. 10b) were originated from $^5D_0 \rightarrow {}^7F_1$, $^5D_0 \rightarrow {}^7F_2$,
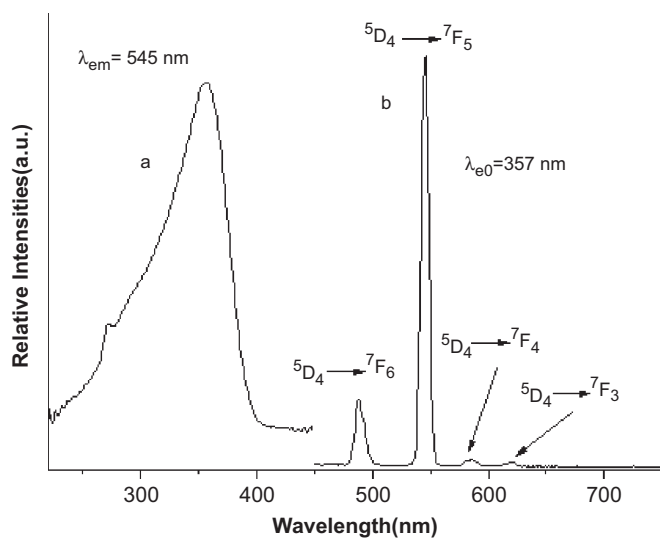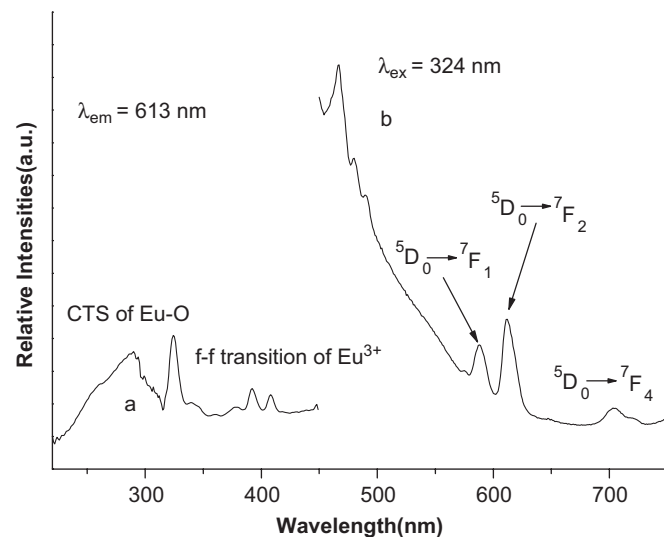

Fig. 10. Excitation (a) and emission (b) spectra of Eu-MMBA-MCM-41 hybrid material.

$^5D_0 \rightarrow {}^7F_4$ transitions at 589, 613, and 703 nm of Eu^{3+}. The $^5D_0 \rightarrow {}^7F_2$ transition is a typical electric dipole transition and strongly varies with the local symmetry of Eu^{3+} ions, while the $^5D_0 \rightarrow {}^7F_1$ transition corresponds to a parity-allowed magnetic dipole transition, which is practically independent of the host material. In addition, among these transitions, $^5D_0 \rightarrow {}^7F_2$ transition shows the strongest red emission, suggesting the chemical environment around Eu^{3+} ions is in low symmetry [41]. Compared with the pure $Eu(MMBA)_3$ complex(Fig. 11b), the excitation band becomes narrower and the maximum excitation wavelength shifts from 395 to 324 nm. The blue-shift of the excitation bands as the introduction of Eu^{3+} complex into the mesoporous material is due to a hypsochromic effect resulting from the change in the polarity of the environment surrounding the Eu^{3+} complex in the mesoporous material [30]. The high baseline in the left emission region (Fig. 10b) corresponded to the Si–O network in the host matrix, indicating that the energy transfer from MMBA-Si to Eu^{3+} is not effective. As a consequence, Eu^{3+} ion covalently bonded hybrid mesoporous material cannot give the same high-emission intensities as Tb-MMBA-MCM-41, showing that the modified ligand MMBA-Si is the most efficient for Tb^{3+} ion and could sensitize its corresponding green emission due to the proper energy level match (Fig. 12).

The typical decay curve of the Tb and Eu mesoporous hybrid materials (Fig. 11a and b) were measured with the excitation wavelength at 340 nm and the emission wavelength at 545 nm for Tb mesoporous hybrid material and 613 nm for Eu mesoporous hybrid material, respectively. The decay curves can be described as a single exponential $(Ln(S(t)/S_0) = -k_1 t = -t/\tau)$, indicating that all Eu^{3+} and Tb^{3+} ions occupy the same average coordination environment. The resulting lifetimes of Tb^{3+} and Eu^{3+} hybrids were given in Table 2. Furthermore, we
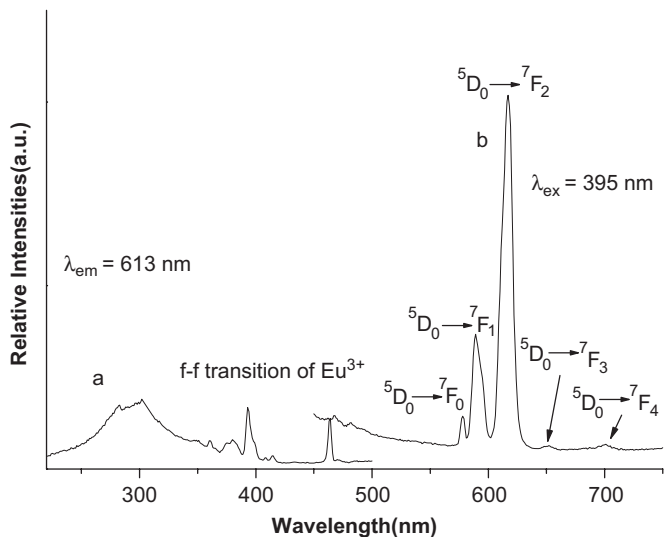

Fig. 9. Excitation (a) and emission (b) spectra of pure $Tb(MMBA)_3$ complex.

Fig. 11. Excitation (a) and emission (b) spectra of pure Eu(MMBA)$_3$ complex.
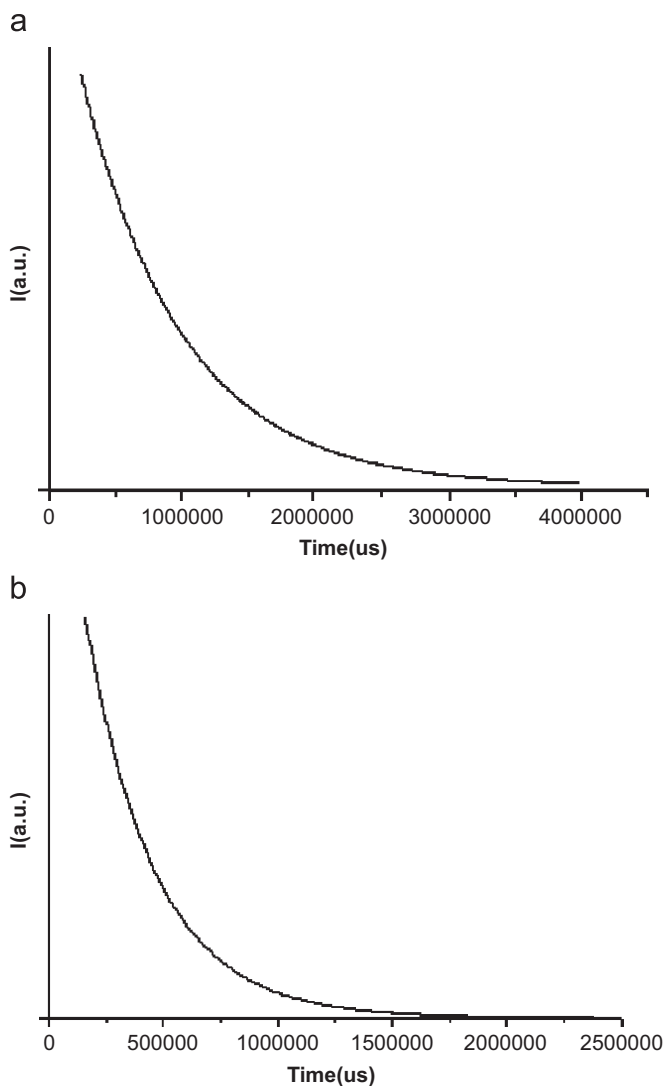

Fig. 12. Decay curves of Tb-MMBA-MCM-41 (a) and Eu-MMBA-MCM-41 (b) hybrid materials.

selectively determined the emission quantum efficiencies of the $^5D_0$ europium ion excited state for Eu^{3+} hybrids on the basis of the emission spectra and lifetimes of the $^5D_0$ emitting level using the four main equations according to Refs. [42–47]. The detailed principle and method was adopted from Ref. [48] and the data were shown in Table 2:

$$A_{0J} = A_{01}(I_{0J}/I_{01})(v_{01}/v_{0J}),$$ (1)

$$A_{rad} = \Sigma A_{0J} = A_{00} + A_{01} + A_{02} + A_{03} + A_{04},$$ (2)

$$\tau = A_{rad}^{-1} + A_{nrad}^{-1},$$ (3)

$$\eta = A_{rad}/(A_{rad} + A_{nrad}).$$ (4)

Here A_{0J} is the experimental coefficients of spontaneous emissions, among A_{01} is the Einstein's coefficient of spontaneous emission between the $^5D_0$ and $^7F_1$ energy levels, which can be determined to be $50\,s^{-1}$ approximately [48] and as a reference to calculate the value of other A_{0J}. I is the emission intensity and can be taken as the integrated intensity of the $^5D_0 \rightarrow {}^7F_J$ emission bands [43,44]. v_{0J} refers to the energy barrier and can be determined from the emission bands of Eu^{3+}'s $^5D_0 \rightarrow {}^7F_J$ emission transitions. A_{rad} and A_{nrad} mean to the radiative transition rate and nonradiative transition rate, respectively, among A_{rad} can be determined from the summation of A_{0J} (Eq. (2)). On the basis the above equation, the luminescence quantum efficiency can be calculated from the luminescent lifetime, radiative, and nonradiative transition rate. The covalently bonded hybrid material Eu-MMBA-MCM-41 possesses the low quantum efficiency of 4.5%, further suggesting the unsuitable energy match and ineffective energy transfer in this hybrid system.

4. Conclusion

In summary, the lanthanide (Tb^{3+}, Eu^{3+}) complexes have been successfully covalently immobilized in the ordered MCM-41 mesoporous material by the modification of *meta*-methylbenzoic acid (MMBA) group with 3-(triethoxysilyl)-propyl isocyanate (TEPIC) using a co-condensation method. The synthesis of MMBA-MCM-41 provides a convenient approach of tailoring the surface properties of mesoporous silicates by organic functionalization, and the derivative materials *Ln*-MMBA-MCM-41 (*Ln* = Tb, Eu) all retain the ordered mesoporous structures. Further investigation into the luminescence properties of *Ln*-MMBA-MCM-41 mesoporous materials show that the characteristic luminescence of the corresponding lanthanide ions (Ln^{3+}) through the intramolecular energy transfers from the modified ligand to the lanthanide ions. Meantime, the luminescent lifetime of two mesoporous materials indicates the similar feature to the luminescence intensities, elucidating that the triple state energy level of MMBA-Si is more quite suitable for the central Tb^{3+} than Eu^{3+}. Moreover, compared with the pure rare-earth

Table 2
Photoluminescent data of *Ln*-MMBA-MCM-41 (*Ln* = Tb, Eu)

	λ_{em} (nm)	I (a.u.)	T (ms)	$1/\tau$ (m/s)	A_r (m/s)	A_{nr} (m s)	η (%)	n_w
Tb-MMBA-MCM-41	486	444.77	0.76	1.315	–	–	–	–
	543	645.00						
	580	133.37						
	612	156.25						
Eu-MMBA-MCM-41	589	622.90	0.31	3.230	0.15	3.08	4.5	3
	613	475.02						
	708	583.04						

complex doped with organic ligand MMBA, the thermal stabilities and photophysical properties of the lanthanide complexes will be improved by the host matrix MCM-41.

Acknowledgment

References

[1] G. Blasse, J. Alloy Compd. 225 (1995) 529–533.
[2] J.M. Lehn, Angew. Chem. Int. Ed. Engl. 29 (1990) 1304–1308.
[3] B. Yan, Y.S. Song, J. Fluoresc. 14 (2004) 289–294.
[4] Y.S. Song, B. Yan, Z.X. Chen, J. Solid State Chem. 177 (2004) 3805–3814.
[5] B. Yan, B. Zhou, J. Photochem, Photobiol. A. Chem. 171 (2005) 181–186.
[6] C.M. Leu, Z.W. Wu, K.H. Wei, Chem. Mater. 14 (2002) 3016–3021.
[7] M. Nandi, J.A. Conklin, L. Salvati, A. Sen, Chem. Mater. 2 (1990) 772–776.
[8] P.A. Tanner, B. Yan, H.J. Zhang, J. Mater. Sci. 35 (2000) 4325–4328.
[9] N.I. Koslova, B. Viana, C. Sanchez, J. Mater. Chem. 3 (1993) 111–112.
[10] C. Sanchez, B. Lebeau, Mater. Res. Soc. Bull. 26 (2001) 377–395.
[11] H.R. Li, J. Lin, H.J. Zhang, L.S. Fu, Chem. Mater. 14 (2002) 3651–3655.
[12] H.R. Li, J. Lin, H.J. Zhang, L.S. Fu, Chem. Commun. (2001) 1212–1213.
[13] P. Lenaerts, K. Driesen, R.V. Deun, K. Binnemans, Chem. Mater. 17 (2005) 2148–2154.
[14] L.D. Carlos, R.A. Sa. Ferreira, R.N. Pereira, M. Assuncao, V. de Zea. Bermudez, J. Phys. Chem. B 108 (2004) 14924–14932.
[15] L.D. Carlos, R.A. Sa. Ferreira, J.P. Rainho, V. de Zea. Bermudez, Adv. Funct. Mater. 12 (2002) 819–823.
[16] D.W. Dong, S.C. Jiang, Y.F. Men, X.L. Ji, B.Z. Jiang, Adv. Mater. 12 (2000) 646–649.
[17] A.C. Franville, D. Zambon, R. Mahiou, Chem. Mater. 12 (2000) 428–435.
[18] Q.M. Wang, B. Yan, J. Mater. Chem. 2004 14 (2002) 2450–2455.
[19] Q.M. Wang, B. Yan, Cryst. Growth Des. 5 (2002) 497–503.
[20] Q.M. Wang, B. Yan, J. Organomet. Chem. 691 (2006) 540–545.
[21] J. Yu, J.L. Shi, L.Z. Wang, M.L. Ruan, D.S. Yan, Mater. Lett. 48 (2001) 112–116.
[22] T. Maschmeyer, F. Rey, G. Sankar, J.M. Thomas, Nature 378 (1995) 159–162.
[23] R. Burch, N. Cruise, D. Gleeson, S.C. Tsang, Chem. Commun. (1996) 951–952.
[24] D.J. MacQuarrie, Chem. Commun. (1996) 1961–1962.
[25] C.E. Fowler, S.L. Burkett, S. Mann, Chem. Commun. (1997) 1769–1770.
[26] M. Sasidharan, N.K. Mal, A. Bhaumik, J. Mater. Chem. 17 (2007) 278–283.
[27] K. Binnemans, P. Lenaerts, K. Driesen, C. Gorller-Walrand, J. Mater. Chem. 14 (2004) 191–195.
[28] H.R. Li, J. Lin, L.S. Fu, J.F. Guo, Q.G. Meng, F.Y. Liu, H.J. Zhang, Micropor. Mesopor. Mater. 55 (2002) 103–107.
[29] L.N. Sun, J.B. Yu, H.J. Zhang, Q.G. Meng, E. Ma, C.Y. Peng, K.Y. Yang, Micropor. Mesopor. Mater. 98 (2007) 156–165.
[30] C.Y. Peng, H.J. Zhang, J.B. Yu, Q.G. Meng, L.S. Fu, H.R. Li, L.N. Sun, X.M. Guo, J. Phys. Chem. B 109 (2005) 15278–15287.
[31] Q.M. Wang, B. Yan, J. Mater. Res. 20 (2005) 592–598.
[32] J.S. Beck, J.C. Vartuli, W.J. Roth, M.E. Leonowicz, C.T. Kresge, K.D. Schmitt, C.T. Chu, D.H. Olson, E.W. Sheppard, S.B. McCullen, J.B. Higgins, J.L. Schlenker, J. Am. Chem. Soc. 114 (1992) 10834–10843.
[33] J.Y. Zhang, Z. Luz, D. Goldfarb, J. Phys. Chem. B. 101 (1997) 7087–7094.
[34] D.H. Everett, Pure Appl. Chem. 31 (1972) 577–638.
[35] K.S.W. Sing, D.H. Everett, R.A.W. Haul, L. Moscow, R.A. pierotti, J. Rouquerol, T. Siemieniewska, Pure Appl. Chem. 57 (1985) 603–619.
[36] M.H. Lim, A. Stein, Chem. Mater. 11 (1999) 3285–3295.
[37] W.H. Zhang, X.B. Lu, J.H. Xiu, Z.L. Hua, L.X. Zhang, M. Robertson, J.L. Shi, D.S. Yan, J.D. Holmes, Adv. Funct. Mater. 14 (2004) 544–552.
[38] C.Y. Peng, H.J. Zhang, Q.G. Meng, H.R. Li, J.B. Yu, F.J. Guo, L.N. Sun, Inorg. Chem. Commun. 8 (2005) 440–443.
[39] Q.Y. Hu, J.E. Hampsey, N. Jiang, C.J. Li, Y.F. Lu, Chem. Mater. 17 (2005) 1561–1569.
[40] M.V. Landau, S.P. Parkey, M. Herskowitz, O. Regev, S. Pevzner, T. Sen, Z. Luz, Micropor. Mesopor. Mater. 33 (1999) 149–1263.
[41] X.M. Guo, L.S. Fu, H.J. Zhang, L.D. Carlos, C.Y. Peng, J.F. Guo, J.B. Yu, R.P. Deng, L.N. Sun, New J. Chem. 29 (2005) 1351–1358.
[42] O.L. Malta, M.A. Couto dos Santos, L.C. Thompson, N.K. Ito, J. Lumin. 69 (1996) 77–84.
[43] O.L. Malta, H.F. Brito, J.F.S. Menezes, F.R Gonçalves e Silva, Alves, F.S. Farias, A.V.M. Andrade, J. Lumin. 75 (1997) 255–268.
[44] L.D. Carlos, Y. Messaddeq, H.F. Brito, R.A. Sa′ Ferreira, V. deZea Bermudez, S.J.L. Ribeiro, Adv. Mater. 12 (2000) 594–598.
[45] R.A. Sa′ Ferreira, L.D. Carlos, R.R. Gonçalves, S.J.L. Ribeiro, V. de Zea Bermudez, Chem. Mater. 13 (2001) 2991–2998.
[46] P.C.R. Soares-Santos, H.I.S. Nogueira, V. Fe′lix, M.G.B. Drew, R.A. Sa′ Ferreira, L.D. Carlos, T. Trindade, Chem. Mater. 15 (2003) 100–108.
[47] E.E.S. Teotonio, J.G.P. Espy′nola, H.F. Brito, O.L. Malta, S.F. Oliveria, D.L.A. de Foria, C.M.S. Izumi, Polyhedron 21 (2002) 1837–1844.
[48] M.H.V. Werts, R.T.F. Jukes, J.W. Verhoeven, Phys. Chem. Chem. Phys. 4 (2002) 1542–1548.